Large-scale filament formation inhibits the activity of CTP synthetase

Rachael Barry, Anne-Florence Bitbol, Alexander Lorestani, Emeric J Charles, Chris H Habrian, Jesse M Hansen, Hsin-Jung Li, Enoch P Baldwin, Ned S Wingreen, Justin M Kollman, Zemer Gitai

DOI: http://dx.doi.org/10.7554/eLife.03638

Cite as: eLife 2014;10.7554/eLife.03638

Received: 9 June 2014
Accepted: 15 July 2014
Published: 16 July 2014

Large-scale filament formation inhibits the activity of CTP synthetase

Rachael M. Barry[1], Anne-Florence Bitbol[2], Alexander Lorestani[1], Emeric J. Charles[3], Chris H. Habrian[4], Jesse M. Hansen[3], Hsin-Jung Li[1], Enoch P. Baldwin[4], Ned S. Wingreen[1,2], Justin M. Kollman[3,5], Zemer Gitai[1]*

[1] Department of Molecular Biology, Princeton University, Princeton, NJ 08544

[2] Lewis-Sigler Institute for Integrative Genomics, Princeton University, Princeton, NJ 08544

[3] Department of Anatomy and Cell Biology, McGill University, Montreal, Quebec

[4] Department of Molecular and Cellular Biology, University of California, Davis

[5] Groupe de Recherche Axé sur la Structure des Protéines, McGill University, Montreal, Quebec

-
- * Please address correspondence to zgitai@princeton.edu
-

Competing Interests

The authors have declared that no competing interests exist.

Impact Statement

A new enzymatic control paradigm: the function, mechanism, and logic of CtpS regulation by large-scale polymerization.

Summary

CTP Synthetase (CtpS) is a universally conserved and essential metabolic enzyme. While many enzymes form small oligomers, CtpS forms large-scale filamentous structures of unknown function in prokaryotes and eukaryotes. By simultaneously monitoring CtpS polymerization and enzymatic activity we show that polymerization inhibits activity and CtpS's product, CTP, induces assembly. To understand how assembly inhibits activity, we used electron microscopy to define the structure of CtpS polymers. This structure suggests that polymerization sterically hinders a conformational change necessary for CtpS activity. Structure-guided mutagenesis and mathematical modeling further indicate that coupling activity to polymerization promotes cooperative catalytic regulation. This previously-uncharacterized regulatory mechanism is important for cellular function since a mutant that disrupts CtpS polymerization disrupts *E. coli* growth and metabolic regulation without reducing CTP levels. We propose that regulation by large-scale polymerization enables ultrasensitive control of enzymatic activity while storing an enzyme subpopulation in a conformationally restricted form that is readily activatable.

Introduction

Many enzymes form small-scale oligomers with well-defined subunit numbers, typically ranging from 2-12 subunits per oligomer. Recent studies suggest that some enzymes can also form large, higher-order polymers in which dozens to hundreds of subunits assemble into filaments (Barry and Gitai, 2011). For most of these structures we lack an understanding of both the regulation and functional significance of their polymerization. To address these questions we focused on the assembly of CTP synthetase (CtpS), an essential and universally conserved metabolic enzyme. CtpS forms large, micron-scale filaments in a wide variety of bacterial and eukaryotic species (Ingerson-Mahar et al., 2010; Liu, 2010; Noree et al., 2010), but the structure of these polymers, what triggers their formation, and the relationship between CtpS polymerization and enzymatic activity were unknown until now.

Cellular CTP levels are subject to exquisitely tight homeostatic control, and CtpS is one of the most regulated enzymes in the cell. In both prokaryotes and eukaryotes, CtpS activity is regulated by allosteric control and feedback-inhibition of enzymatic activity, and CtpS levels are regulated by transcriptional and post-translational control (Levitzki and Koshland, 1972b; Long and Pardee, 1967; Meng et al., 2004; Yang et al., 1996). Cells in all kingdoms of life synthesize CTP using CtpS (Long and Pardee, 1967), and its essentiality makes CtpS an attractive chemotherapeutic and antiparasitic target (Hofer et al., 2001; Williams et al., 1978).

The CtpS enzyme has two domains connected by an elongated linker: a glutaminase (GATase) domain that deaminates glutamine and a synthetase (ALase) domain that aminates UTP in an ATP-dependent manner to form CTP. CtpS has binding sites for substrates (glutamine, ATP, and UTP), product (CTP), and a proposed binding site for an allosteric modulator (GTP) (Levitzki and Koshland, 1972b). CtpS tetramerization is necessary for its catalytic activity and is controlled by nucleotide

availability; ATP, UTP, or CTP can favor tetramer formation (Fig. 1A) (Anderson, 1983; Endrizzi et al., 2004; Levitzki and Koshland, 1972a; Pappas et al., 1998). Of critical regulatory importance, CtpS activity is also inhibited by CTP (Long and Pardee, 1967).

Here we determine the function and mechanism of CtpS polymerization. We demonstrate that CtpS polymerization negatively regulates CtpS activity when its CTP product accumulates. We also present the structure of the CtpS polymers and the resulting implications for CtpS inhibition. We confirm the physiological significance of CtpS assembly by demonstrating that polymerization-mediated regulation is essential for the proper growth and metabolism of *E. coli.* Together these findings establish CtpS as a model for understanding enzymatic regulation by large-scale polymerization. Finally, we model how coupling CtpS activity to its large-scale assembly can enable cooperative regulation and discuss the implications of polymerization-based regulation for ultrasensitive metabolic control and cytoskeletal evolution.

Results

CtpS polymerization inhibits enzymatic activity

Because CtpS filament formation is conserved between divergent organisms, we hypothesized that CtpS polymerization may regulate its conserved enzymatic function. We therefore designed a system to simultaneously monitor the assembly and activity of purified *Escherichia coli* CtpS. We used a fluorometer to assay CtpS assembly by right-angle light scattering and CtpS activity by the specific absorbance of its CTP product. CtpS assembly and activity were assayed across a range of enzyme concentrations in activity buffer containing saturating amounts of substrates (UTP, ATP, and glutamine) as well as GTP and Mg^{2+} (referred to as “activity buffer” throughout the text) (Fig. 1B). CtpS protein was first pre-incubated in an incomplete activity buffer without glutamine to favor active tetramer formation. CTP production was then initiated by the addition of glutamine

to form a complete activity buffer. The formation of well-ordered filaments was confirmed by negative stain electron microscopy (EM) (Fig. 1C). Interestingly, at CtpS levels where robust changes in light scattering are observed (above approximately 1-2 μM), CtpS activity (determined by the rate of CTP production per enzyme) sharply decreases (Fig. 1B, Figure 1 supplements 1,2). This abrupt transition in activity state supports the hypothesis that there is a threshold for polymerization and that polymerization is inhibitory. Noise and nonlinearity in the light scattering data make it difficult to determine an exact critical concentration value. However, based on correlation between light scattering and CTP production changes, we predict the assembly threshold of CtpS to be approximately 1-2 μM. The cellular level of CtpS protein in *E. coli* grown in minimal media was measured at 2.3 μM (Fig. 1, supplement 3), indicating that the CtpS polymerization observed *in vitro* may be physiologically favorable.

To determine if polymerization indeed inhibits CtpS activity, we assayed the activity of polymers purified by ultracentrifugation. The polymer-containing pellet was least enzymatically active immediately after centrifugation and CtpS activity increased as the polymers in the pellet disassembled (Fig. 1D; Fig. 1, supplements 4,5). CtpS polymers are thus inactive or much less than maximally active and polymerization is readily reversible. We directly demonstrated the reversibility of CtpS assembly and inactivation by first allowing CtpS to polymerize in activity buffer (with all substrates present) and then adding 1 mM UTP and ATP. Upon addition of these substrate nucleotides, we observed a sharp decrease in light scattering that corresponded to a sharp increase in CtpS activity. This transition was followed by a gradual increase in light scattering and corresponding decrease in activity back to the initial residual level (Fig. 1E). Control experiments confirmed that the decrease in CtpS polymerization was not due to mechanical disruption by substrate addition (Fig. 1, supplement 6). The correlation between the decrease in light scattering and the initiation of CTP production

128 at the time of substrate addition indicates that substrate addition leads to rapid
129 depolymerization and subsequent enzyme reactivation. Immediately after this point, we
130 observed an increase in both CTP levels and polymerization. We therefore conclude that
131 polymerized CtpS enzymes are inactive and must disassociate from the polymer to
132 resume normal enzymatic activity. Despite the fact that polymerization occurs in a buffer
133 containing substrates, polymerization only occurs with CTP production, suggesting that
134 polymerization is triggered not by the initial substrates, but rather by the accumulation of
135 CTP product.
136
137 ***CtpS polymerization is induced by its product and repressed by its substrate***
138 In order to identify the factors that control CtpS inhibition by assembly, we first
139 confirmed that none of the substrates alone induced polymerization (Fig. 2, supplement
140 1). We then directly tested our hypothesis that CtpS's product, CTP, a known inhibitor of
141 CtpS activity, stimulates CtpS polymerization. In the absence of substrates (UTP, ATP,
142 and glutamine), incubation with CTP caused CtpS to polymerize (Fig. 2A). The threshold
143 concentration for robust changes in light scattering by CtpS with saturating CTP (1-2 μM
144 CtpS; Fig. 2, supplement 2) agrees with the threshold concentration in the presence of
145 substrates (1-2 μM CtpS; Fig. 1, supplement 1). This result suggests that CTP alone is
146 sufficient to influence polymerization and that the substrates and any other products of
147 the enzymatic reaction are not necessary. To confirm that CTP stimulates CtpS
148 assembly we used ultracentrifugation as an independent assembly assay. Titrating with
149 increasing amounts of CTP caused an increase in the amount of CtpS found in the pellet
150 with respect to the 0 mM CTP condition (Fig. 2B; Fig. 2, supplement 3).
151 We further demonstrated that CTP binding is necessary for polymerization by
152 showing that a $CtpS^{E155K}$ mutant defective for CTP-binding feedback inhibition [reviewed

153 in (Endrizzi et al., 2005)] (Ostrander et al., 1998; Trudel et al., 1984) fails to polymerize
154 under the same CTP-producing conditions in which wild-type enzyme polymerizes (Fig.
155 2C). Furthermore, electron microscopy confirmed that, unlike wild-type CtpS, CtpS^{E155K}
156 does not polymerize in the presence of CTP (Fig. 2D). Together, our data indicate that
157 within our studied range of enzyme concentrations, CtpS's product, CTP, is both
158 necessary and sufficient to induce CtpS polymerization.
159 The CtpS crystal structure suggests that the enzyme's UTP and CTP binding
160 sites partially overlap (Endrizzi et al., 2005), raising the question of whether CtpS
161 assembly is controlled by the absolute level of CTP or the relative product/substrate
162 levels. 6-Diazo-5-oxo-L-norleucine (DON) is a glutamine analog that covalently binds
163 glutaminase active sites and irreversibly inactivates enzymatic activity (Chakraborty and
164 Hurlbert, 1961). When added to activity buffer, DON abolishes both CTP production and
165 CtpS polymerization (Fig. 2, supplement 4). However, DON-treated CtpS can still
166 polymerize when CTP is added to the solution (Fig. 2E). Polymers formed in the
167 presence of CTP and DON disassemble upon the addition of substrates but do not
168 reform after substrate addition (Fig. 2E), presumably because the DON-inhibited CtpS
169 cannot produce additional CTP. DON treatment has no effect on CtpS polymerization
170 when the enzyme is incubated with saturating CTP (Fig. 2, supplements 1, 5). These
171 results suggest that competition between substrate (UTP) and product (CTP) binding
172 controls the polymerization equilibrium of CtpS. The dependence of polymerization on
173 CTP levels may explain why DON treatment abolishes *in vivo* CtpS assembly in some
174 cellular contexts (Ingerson-Mahar et al., 2010) but not others (Chen et al., 2011).
175
176 ***The structure of the CtpS polymer suggests a mechanism for enzymatic inhibition***
177 To better understand the mechanism of enzymatic inhibition by polymerization,
178 we determined the structure of the CtpS filament by cryo-electron microscopy at 8.4 Å

179 resolution (Fig. 3, supplement 1). The repeating subunits of the filament are X-shaped
180 CtpS tetramers (Fig. 3A). The helical symmetry of the filament results in CtpS tetramers
181 stacked atop one another with the arms of the adjacent Xs interdigitated. The 222 point
182 group symmetry of the tetramer is maintained within the filament, resulting in overall
183 twofold symmetry both along and perpendicular to the helical axis. A significant effect of
184 this unusual symmetry is that, unlike many biological polymers, CtpS filaments are
185 apolar.

186 To create an atomic model of the CtpS filament we fit a monomer of the *E. coli*
187 CtpS crystal structure into the cryo-EM structure as three rigid bodies (ALase domain,
188 GATase domain, and the linker region) (Fig. 3B). There is a slight rotation between the
189 GATase and ALase domains, similar to the variation seen across crystal structures of full
190 length CtpS (Fig. 3 supplement 2A). There is strong density for CTP bound at the
191 inhibitory site, and no density in the predicted UTP active site (Fig. 3 supplement 2B),
192 confirming the biochemical data that CTP binding favors assembly. Weaker density is
193 also observed for ADP, but there is no density in the predicted GTP allosteric regulatory
194 site (Fig. 3 supplement 2C,D). There is a minor rearrangement of the tetramerization
195 interface in the filament relative to the crystal structure that results in a compression of
196 the tetramer by about 3 Å along the length of the filament axis (Fig. 4).

197 The cryo-EM structure of the CtpS filament offers insight into the mechanism of
198 enzymatic regulation. All of the enzyme active sites are solvent accessible, suggesting
199 that UTP, ATP and glutamine can freely diffuse into the filament (Fig. 5A). This
200 observation rules out occlusion of active sites as a regulatory mechanism. An alternative
201 mechanism of CtpS inhibition is blocking the transfer of ammonia between the GATase
202 and ALase active sites, which are separated by ~25 Å. The detailed mechanism of
203 ammonia transfer is unknown, but likely involves a conformational rearrangement in the
204 vicinity of a putative channel that connects the two domains (Endrizzi et al., 2004; Goto

205 et al., 2004). One prediction is that a conformational change, induced by UTP and ATP
206 binding, rotates the GATase domain toward the ALase domain to create a shorter
207 channel between the active sites (Goto et al., 2004). Such a large-scale rotation would
208 be unattainable in the steric environment of the filament, as it would lead to clashing of
209 the moving GATase domain with an adjacent CtpS tetramer (Fig. 5B,C). Regardless of
210 the specific changes involved, quaternary constraints imposed by the filament structure
211 likely provide the mechanism for inhibition of the synthesis reaction.
212
213 ***A CtpS polymerization interface mutant disrupts feedback regulation***
214 To validate the filament structure and its mechanistic implications we generated
215 structure-guided mutants in the CtpS polymerization interface. Two discrete segments
216 constitute the novel filament assembly contacts: the linker region α-helix 274-284, and
217 the short α-helix 330-336 of the GATase domain (Fig. 3D,E). Though the exact amino
218 acid sequences at the inter-tetramer assembly interfaces are not well conserved, relative
219 to the rest of CtpS, both sites feature many charged or hydrophobic residues available
220 for potential polymerization stabilization across species (Fig. 6, supplement 1). We
221 previously demonstrated that in *E. coli*, an mCherry-CtpS fusion faithfully reproduces the
222 filamentous localization of native CtpS (as assayed by immunofluorescence) (Ingerson-
223 Mahar et al., 2010). As an initial screen for CtpS assembly, we therefore introduced four
224 mutations in the linker region α-helix and surrounding residues (E277R, F281R, N285D,
225 and E289R) into mCherry-CtpS (Fig. 6A). All four polymerization interface mutants
226 disrupted mCherry-CtpS localization, exhibiting a diffuse localization pattern rather than
227 linear filaments (Fig. 6B).
228 The loss of filamentous mCherry-CtpS localization does not exclude the
229 possibility that the polymerization interface mutants form small filaments that cannot be
230 resolved by light microscopy. Consequently, to determine if the diffuse localization *in*

231 *vivo* reflected a polymerization defect, we purified one of the linker region helix mutants,
232 CtpS^{E277R}, and examined its polymerization by light scattering and EM. CtpS^{E277R} did not
233 significantly polymerize in activity buffer, and no filaments could be detected by EM (Fig.
234 7B; Fig. 7, supplement 1), confirming that CtpS^{E277R} cannot properly polymerize. We
235 attribute the slight linear increase in light scattering with increasing concentration of
236 CtpS^{E277R} to the increase in protein abundance.

237 We next determined the impact of the E277R polymerization interface mutation
238 on CtpS activity. At the lowest protein concentration tested, CtpS^{E277R} exhibited slightly
239 reduced CTP production (71% of wild type maximal activity) compared to the wild type
240 protein (Fig. 7A). To determine if the polymerization defect of CtpS^{E277R} was due to
241 impaired large-scale assembly or reduced CTP production, we used EM to examine its
242 polymerization in the presence of saturating CTP levels. CtpS^{E277R} did not polymerize in
243 the presence of high levels of CTP (Fig. 7B). We thus conclude that CtpS^{E277R} impairs
244 polymerization independently of its effect on activity.

245 Whereas CtpS^{E277R} was slightly impaired in its activity at low enzyme
246 concentrations, CtpS^{E277R} exhibited a much higher concentration at which k_{cat} is one half
247 of its maximum due to polymerization (the $[CtpS]_{0.5}$ value) compared to wildtype CtpS
248 ($[CtpS^{E277R}]_{0.5}$ = 7.1 μM versus $[CtpS]_{0.5}$ = 3.3 μM). Furthermore, the concentration
249 dependence of CtpS^{E277R} k_{cat} was less steep than wildtype, with CtpS^{E277R} retaining 48%
250 of its maximal activity at the highest enzyme concentration tested (8 μM) (Fig. 7A). This
251 behavior was in stark contrast to wild type CtpS, whose activity plummeted to 4% of its
252 maximum. Thus, at low enzyme concentrations, CtpS^{E277R} exhibited slightly lower
253 activity than wild type while at high enzyme concentrations CtpS^{E277R} activity was
254 significantly greater than that of wild type. One explanation for the comparatively modest
255 decrease in CtpS^{E277R} activity as a function of enzyme concentration is that CtpS^{E277R}

256 produces CTP, which at high CtpS concentrations can accumulate and competitively
257 inhibit CtpS activity, resulting in a slight activity decrease. However, this mutant lacks the
258 dramatic reduction in CtpS activity mediated by large-scale assembly into filaments. As
259 predicted from thermodynamic linkage, the inability to polymerize also leads $CtpS^{E77R}$ to
260 bind CTP less tightly, with a higher IC50 value than the wildtype enzyme (830 μM *vs* 360
261 μM at 200 nM enzyme, Fig. 7, supplement 2). These data are thus consistent with the
262 model that CtpS is negatively regulated in two ways: CTP competitively inhibits UTP
263 binding, and large-scale assembly sterically hinders a conformational change required
264 for CtpS activity. The quantitative differences between wild type and $CtpS^{E277R}$ activity
265 suggest that large-scale assembly mediates rapid and efficient inhibition of enzymatic
266 activity.
267
268 ***The $CtpS^{E277R}$ polymerization interface mutant disrupts E. coli growth and***
269 ***metabolism***
270 To determine the impact of $CtpS^{E277R}$ on cell physiology, we replaced wild type
271 CtpS with $CtpS^{E277R}$ at its native locus in *E. coli*. This strain exhibited defective growth
272 compared to wild type in rich (Fig. 7C) and minimal media (Fig. 7, supplement 3). Wild
273 type doubling time was 51 min ± 1.5 min, while the $CtpS^{E277R}$ doubling time was 130 min
274 ± 11 min in rich media. Immunoblotting confirmed that $CtpS^{E277R}$ was expressed at
275 similar levels to wild type CtpS (Fig. 7, supplement 4). One possible explanation for the
276 growth impairment is that $CtpS^{E277R}$ could not produce enough CTP to support robust
277 growth. However, CTP levels, as measured by mass spectrometry, are not reduced in
278 the $CtpS^{E277R}$ strain (Fig. 8, supplement 1). In fact, CTP levels are modestly higher in the
279 mutant than in wild type cells (1.6 ± 0.3 fold higher). Because average CTP levels are
280 higher in these cells, $CtpS^{E277R}$ likely does not impair growth due to reduced CTP

281 production. Rather, the elevated CTP levels and the observation that growth became
282 particularly affected at mid-log phase supports the hypothesis that the CtpS^{E277R} mutant
283 is defective in regulating CTP levels when adapting to changes in the cellular
284 environment.

285 Replacing wild type CtpS with CtpS^{E277R} also affected levels of other nucleotides
286 and their precursors or byproducts (Fig. 8A; Fig. 8, supplement 1). For example, the
287 amount of the pyrimidine precursor orotate was 2.3 $\pm$ 0.5 fold reduced in the mutant,
288 consistent with the idea that CtpS^{E277R} is hyperactive and increases CTP production at
289 the expense of its precursors. Together, these data indicate that disrupting the CtpS
290 polymerization interface does not deplete CtpS or CTP. Instead, we hypothesize that
291 CtpS^{E277R} perturbs *E. coli* growth by disregulating nucleotide metabolism in a manner
292 consistent with hyperactivating CtpS by disrupting a negative regulatory mechanism.
293 These data are consistent with the observation that at the cellular concentration of CtpS,
294 CtpS^{E277R} is more active than the wild type enzyme.
295

296 ***CtpS^{E277R} impairs negative feedback regulation in vivo***

297 Steady-state measurements of metabolite levels cannot establish whether the
298 observed increase in CTP levels corresponds to a defect in feedback inhibition of CtpS
299 (as predicted by our model) or by stimulating CtpS activity in some other way. To directly
300 assess feedback inhibition *in vivo*, we supplemented wild type CtpS or CtpS^{E277R} with
301 C13-labeled cytidine, which is converted into C13-CTP by the nucleotide salvage
302 pathway that functions independently of CtpS (Ayengar et al., 1956; Fricke et al., 1995;
303 Valentin-Hansen, 1978). We note that nucleotide triphosphates cannot be imported into
304 the cell such that we could not supplement with CTP itself. Furthermore, the use of C13-
305 cytidine enabled us to use mass spectrometry to distinguish the CTP produced by
306 nucleotide salvage (C13-CTP) from the CTP produced *de novo* by CtpS (C12-CTP). We

307 hypothesized that if disruption of CtpS polymerization disrupts negative feedback, then
308 CtpS^{E277R} should maintain high CtpS activity despite the accumulation of C13-CTP from
309 supplementation with C13-cytidine.

310 As predicted based on the independence of nucleoside import from nucleotide
311 biosynthesis, the incorporation of C13-label into the CTP pool was similar in the wild
312 type and CtpS^{E277R} strains, indicating that both take up labeled cytidine and convert it
313 into CTP at approximately the same rate (Fig. 8B). In wild type cells, as the C13-CTP
314 pool increased, the fraction of C12-CTP sharply decreased (Fig. 8C). Thus, feedback
315 regulation mechanisms compensate for the increased CTP production from cytidine by
316 reducing *de novo* CTP production by CtpS. The decrease in the fraction of unlabeled
317 CTP was less pronounced in the CtpS^{E277R} mutant and by the end of the period assayed,
318 unlabeled CTP levels were almost twofold higher in the CtpS^{E377R} strain than in wild type
319 (Fig. 8, supplement 2). This result supports our conclusion that CtpS^{E277R} hyperactivates
320 CtpS by disrupting its negative feedback regulation and that this hyperactivation more
321 than compensates for its reduced enzymatic activity. Since disruption of just one
322 interaction in the proposed polymerization interface weakened the ability of CtpS to
323 control CTP production even when all other forms of CtpS regulation are unaltered, we
324 predict that any disruption of regions of inter-tetrameric contact, either by changes to the
325 protein sequence or by chemical perturbation, would cause this deleterious regulatory
326 defect.

327

328 ***Coupling activity to polymerization enables ultrasensitive enzymatic regulation***

329 What is the benefit of using polymerization as a negative-feedback regulation
330 strategy? To quantitatively assess the impact of polymerization-mediated enzymatic
331 inhibition, we developed a simple mathematical model of CtpS inhibition by CTP-
332 dependent polymerization (see Supplementary Material for details). A key point of the

333 model is that the concentration of CtpS needed for polymerization depends on the free
334 energy of polymerization, which in turn depends on the UTP and CTP concentrations.
335 One mechanism for how CTP induces reversible polymerization is by CTP binding more
336 favorably to the filament than to the free tetramer. This model leads to two predictions
337 dictated by thermodynamic linkage: 1) CTP should be a more effective inhibitor at CtpS
338 concentrations that favor polymer formation, and 2) the presence of CTP should
339 enhance polymer formation and the reduction in CtpS specific activity (k_{cat}) as CtpS
340 concentration increases. Indeed, At 4 μM CtpS, near the concentration at which CtpS
341 k_{cat} is one half of its maximum due to polymerization ($[CtpS]_{0.5}$, 3.3 μM, Fig. 7A), the CTP
342 IC50 value is reduced to 170 μM, compared to 360 μM at 200 nM enzyme (Fig. 7,
343 supplement 2). Conversely, in the presence of 800 μM CTP, the $[CtpS_{0.5}]$ value is 1.4
344 μM, reduced by more than half compared to that with no CTP (Fig. 7, supplement 3).
345 Interestingly, the presence of 400 μM CTP has only a small effect ($[CtpS]_{0.5}$ = 2.8 μM) ,
346 suggesting an ultrasensitive response of polymerization to CTP levels.
347 Another result of this polymerization-based mechanism is that the cooperativity of
348 CTP-mediated inhibition increases as a function of the nucleation barrier to
349 polymerization. Experimentally, the abundance of long polymers in vitro (Fig. 1B) and
350 the small number of polymers per cell in vivo (Ingerson-Mahar et al., 2010) suggest that
351 CtpS polymerization exhibits a significant nucleation barrier. The conformational
352 differences between the free and filament forms of CtpS (Fig. 4) may play a role in
353 establishing this barrier. This barrier could result from the free energy change required to
354 take the CtpS tetramer from a flexible “free” state to more rigid “filament” state upon the
355 first assembly step of the polymer. Alternatively, dimerization of “free” CtpS tetramers
356 could allosterically influence one another to adopted the “filament” conformation in a
357 manner similar to one proposed for the cooperative polymerization of FtsZ (Miraldi et al.,

2008). Our mathematical model enables us to estimate this nucleation barrier from the average polymer length, yielding a value of order 9 k_BT, where k_BT is the thermal energy. Moreover, it demonstrates that coupling activity to polymerization with such a significant nucleation barrier represents a mechanism for generating extremely sharp transitions in enzyme activity.

We compared the sharpness of enzyme inhibition in our novel polymerization-based mechanism to that of previously-characterized mechanisms of enzyme inhibition such as competitive and allosteric inhibition (Fig. 8D, Supplementary File 1). We found that, among the mechanisms examined, the ones involving polymerization-based negative feedback yield the sharpest decrease in enzyme activity when CTP levels are increased, thereby enabling tight regulation of CTP production by CTP levels. Our estimate based on average CtpS filament length of the value of the nucleation energy yields extremely sharp transitions (see Fig. 8D, where this estimate was used, and our discussion of response coefficients in Supplementary File 1). This sharpness is apparent in comparing the concentration dependences of CtpS specific activity in the presence of CTP. The $CTPS_{0.5}$ value at 400 μM CTP is slightly shifted compared to no CTP, to that at 800 μM where the $CTPS_{0.5}$ value is substantially decreased and the curvature more concave (Fig. 8, supplement 3).

Because the onset of the decrease of activity can become arbitrarily sharp as the nucleation energy is increased, polymerization-mediated regulation is fundamentally different from the case of fixed stoichiometry enzyme oligomers, such as hemoglobin, that cooperatively bind an inhibitor. Another crucial difference with respect to such simple cooperative inhibition is that the polymerization-based mechanism also mediates negative feedback on CtpS activity from CtpS levels (see Supplementary File 1). Hence, this mechanism uniquely enables ultrasensitive regulation of CtpS activity by both CTP

383 and CtpS concentrations. Additionally, sequestering CtpS tetramers into the inactive
384 filament ensures the availability of a CtpS pool that can be rapidly reactivated, limited
385 only by the polymer disassembly rate. Our biochemical data confirms that
386 depolymerization and subsequent repolymerization can occur within seconds (Fig. 1E),
387 while investigation the *in vivo* kinetics of CtpS filament assembly and disassembly
388 presents an interesting subject for future study.
389
390 **Discussion**
391 Our studies suggest that in addition to being regulated by small-scale
392 oligomerization, allosteric control, competitive inhibition, and transcriptional and post-
393 translational mechanisms, CtpS is also regulated by large-scale assembly into filaments
394 comprising hundreds of subunits (Fig. 1C). CtpS polymerization is cooperative, which we
395 conclude based on light scattering dynamics, the long polymers observed by EM, and
396 the large fraction of polymerized protein observed by sedimentation (if assembly were
397 non-cooperative one should always observe more tetramers than polymers). CtpS
398 polymerization inhibits CtpS activity. The polymerization of CtpS is stimulated by binding
399 its product, CTP, and disrupted by binding its substrates, UTP and ATP (Fig. 1E, 9).
400 Inter-tetramer interactions in the CtpS polymer sterically inhibit a conformational change
401 that is thought to be necessary for CtpS activity, and mutations that disrupt
402 polymerization disrupt CtpS regulation with significant impacts on cell growth and
403 metabolism.
404
405 ***The benefits of harnessing polymerization as a regulatory mechanism***
406 With so many regulatory strategies in place, why add another? First, layering
407 multiple levels of regulation results in robust regulatory control with a series of fail-safes
408 that protect the cell from disregulated nucleotide levels. CtpS is a key node in nucleotide

409 metabolism because it binds ATP, UTP, CTP, and GTP. We propose that strict
410 regulation of nucleotide levels is so critical to controlled growth and division that CtpS
411 evolved as a master switch to integrate information about nucleotide abundances and
412 maintain their proper levels and proportions. Nucleotide biosynthesis is both
413 energetically costly and controls the availability of raw materials for replication,
414 transcription, and other biosynthetic pathways. Thus, coordinating biomass accumulation
415 and cellular proliferation requires the extremely tight control of nucleotide levels via CtpS
416 that no one regulatory mechanism could achieve on its own. The need for such tight
417 regulation could also explain recent observations that small CtpS polymers can combine
418 to form higher-order larger structures (Gou et al., 2014) and can co-localize with other
419 proteins involved in nucleotide metabolism [reviewed in (Carcamo et al., 2014)].
420 The second advantage of employing multiple types of regulation is that each
421 regulatory strategy has distinct kinetics that together enable regulation over a wide range
422 of potential conditions. For example, transcriptional regulation is slow in comparison to
423 regulation by ligand binding. Competitive or allosteric regulation by ligand binding can be
424 cooperative if the enzymes form oligomers, as in the case of hemoglobin (Perutz, 1989).
425 However, the amassed activity of such oligomers is strictly linear with respect to protein
426 concentration. By contrast, our modeling indicates that coupling activity to ligand-
427 induced polymerization is a simple mechanism for promoting cooperativity with respect
428 to protein concentration, while at the same time maintaining cooperativity with respect to
429 ligand binding. An added benefit of polymerization-mediated inhibition is that it enables
430 cells to sequester CtpS in an activity-primed tetramer state such that CtpS can be rapidly
431 reactivated in a manner limited only by enzyme depolymerization (Fig. 9). Previous
432 models for enzyme sequestration have relied on the idea of preventing substrate binding
433 [e.g., (Jackson-Fisher et al., 1999; Michaelis and Gitai, 2010)]. Here we propose an
434 alternate mechanism for sequestration where the active sites can readily access

435 substrates but conformational changes required for activity are restricted. While our data
436 are consistent with the model of cooperative regulation by assembly, experimental noise
437 and nonlinearities limit the current ability to measure the extent of that cooperativity,
438 raising the possibility that there are yet more undiscovered features of CtpS regulation.
439 As methods for manipulating and monitoring nucleotide levels become more available, it
440 will also be interesting to determine the kinetics of the various CtpS regulatory
441 mechanisms *in vivo*.
442
443 ***Do other enzymes utilize polymerization-based regulation?***
444 Though we have only tested the *E. coli* CtpS enzyme, we hypothesize that other
445 prokaryotic and eukaryotic CtpS proteins may be subject to inhibition by polymerization.
446 *C. crescentus* CtpS disassembles in the presence of DON while *S. cerevisiae* CtpS
447 shows longer filaments when cells were exposed to additional CTP (Ingerson-Mahar et
448 al., 2010; Noree et al., 2010). The linker region implicated in *E. coli* CtpS polymerization
449 is also mutated in three independent human lung carcinoma samples (Forbes et al.,
450 2008), suggesting that metabolic regulation by CtpS polymerization is important for
451 limiting human cell proliferation.
452 In the future it will be interesting to determine if other enzymes employ
453 polymerization-mediated regulatory strategies. In particular, we predict that enzymes
454 that function at key metabolic nodes would most benefit from the ultrasensitive
455 regulation provided by polymerization. Such cooperative assembly can coordinate the
456 mobilization or sequestration of functional units, thereby dynamically altering the level of
457 active enzyme without altering the overall enzyme concentration. The ultrasensitive
458 kinetics of this transition would allow for cells to rapidly respond to short-term changes in
459 their environment or metabolic needs. For example, immediately following cell division,
460 daughter cells could depolymerize any CtpS filaments inherited to compensate for

461 reduced CtpS concentrations (perhaps from unequal partitioning) faster than translating
462 and folding new proteins. The rapid kinetics of polymerization could sequester CtpS
463 when CTP is plentiful to prevent futile biosynthesis. A handful of other metabolic
464 enzymes have been shown to form filamentous or large scale structures *in vitro* and *in*
465 *vivo* (Barry and Gitai, 2011). CtpS may thus emerge as a model for a larger class of
466 enzymes that are regulated by higher-order assembly to achieve cooperative enzyme
467 activation or inactivation.
468
469 ***Enzymatic regulation may have driven the evolution of large-scale polymers***
470 Large-scale polymers such as cytoskeletal filaments play an essential role in
471 organizing the cell. But how did such cytoskeletal polymers evolve? Our findings suggest
472 that the selective benefit conferred by improving enzymatic regulation may have led to
473 the evolution of large-scale filaments. Once present, these enzymatic polymers could
474 then be appropriated for the structural functions commonly associated with the
475 cytoskeleton. Finally, gene duplication and divergence would enable uncoupling and
476 specialization of the enzymatic and structural properties of these proteins (Barry and
477 Gitai, 2011).
478 The observation that CtpS polymerization is conserved among diverse
479 prokaryotes and eukaryotes supports the hypothesis that CtpS polymerization arose in
480 an early common ancestor and is a key feature of CtpS regulation. An example of
481 appropriating an enzymatic polymer for structural functions comes from *Caulobacter*
482 *crescentus*, where CtpS filaments regulate cell shape in a manner that can be uncoupled
483 from their enzymatic activity (Ingerson-Mahar et al., 2010). While the enzymatic activity
484 and polymerization capacity of CtpS is universally conserved, its cell shape function
485 appears to be species-specific. Thus, polymerization appears to have evolved early to

regulate enzymatic activity while CtpS polymers were only later adapted for a structural role.

A similar evolutionary path could explain the structural similarity between hexokinase enzymes and the actin family of cytoskeletal elements (Holm and Sander, 1993; van den Ent et al., 2001). Specifically, we hypothesize that actin and hexokinase may have shared a common ancestor that, like CtpS, evolved polymerization as a regulatory mechanism. Gene duplication and divergence may have subsequently enabled actin to specialize as a structural element, while additional layers of enzymatic regulation may have obviated the need for hexokinase assembly (mammalian hexokinase does not polymerize). In this way, CtpS assembly and regulation may provide insight into the origins of the intracellular structural network that became the modern cytoskeleton.

500 **Materials and Methods**

501 ***E. coli* strains**

Strain	Description	Reference
ZG247	NCM3722	(Soupene et al., 2003)
ZG1075	pyrG-His in BL21 * (DE3)	(Ingerson-Mahar et al., 2010)
ZG1076	pyrG^{E155K}-His in BL21 * (DE3)	This study.
ZG1077	pyrG^{E277R}-His in BL21 * (DE3)	This study.
ZG1082	mCherry-CtpS in NCM3722	(Ingerson-Mahar et al., 2010)
ZG1083	mCherry-CtpS^{E277R} in NCM3722	This study.
ZG1084	mCherry-CtpS^{F281R} in NCM3722	This study.
ZG1085	mCherry-CtpS^{N285D} in NCM3722	This study.
ZG1086	mCherry-CtpS^{E289R} in NCM3722	This study.
ZG1168	CtpS^{E277R}-kan^{R} chromosomal integrant in NCM3722	This study.
ZG1169	WT-kan^{R} chromosomal integrant in NCM3722	This study.

502

503 **CtpS purification**

504 Wild type CtpS was purified as described previously (Ingerson-Mahar et al., 2010).
505 CtpS-E155K and CtpS-E227R were purified as described previously with the exception
506 that the 6XHis affinity tag was not cleaved in these cases. Similar treatment of the wild
507 type protein proved indistinguishable from the cleaved sample.

508

509 **Activity/polymerization assay**

510 Purified CtpS protein was incubated at 37° C for 20 min in 50 mM Tris HCl (pH 7.8), 10
511 mM $MgCl_2$, 1 mM UTP, 1 mM ATP, and 0.2 mM GTP to allow tetramer formation. CTP
512 production was initiated by the addition of 10 mM glutamine to create a full activity buffer
513 (referred to in text at "activity buffer") (Ingerson-Mahar et al., 2010) immediately prior to
514 recording of sample measurements. Time between glutamine addition and initiation of
515 sample recording averaged 5 seconds and was based on the amount of time required to
516 load the sample. Reaction was monitored at 37° C for 5 minutes in a Photon
517 Technology International QuantaMaster 40 Fluorometer equipped with photo multiplier
518 tubes for both scattering and transmittance. Right angle light scattering at 405 nm with a
519 1 mM slit width detected polymerization, and transmittance at 291 nm with a 0.25 mM slit
520 width detected CTP production with both values reported in arbitrary units. Reactions
521 were performed in 150 µl samples. Polymerization was monitored for 3 minutes unless
522 otherwise noted. Detection of light scattering and transmittance alternated with an
523 integration time of 1 second. CTP production velocity (k_{cat}, µmol/s) was determined for
524 the first 30 seconds of the reaction. CTP production was normalized by the
525 concentration of CtpS enzyme in each sample. Due to the fluorometer assay's use of
526 transmittance and a photon multiplier, we compared data collected to data collected over
527 the same concentration range on a more traditional spectrophotometer setup in the
528 Baldwin lab. Comparison yielded the presence of a scaling factor to be applied to the
529 fluorometer data set to yield k_{cat} ranges consistent with published data. Data were
530 scaled to yield the same maximal k_{cat} value for both data sets. The fold-change in
531 activity over the concentrations was similar between the data sets. Overlay of the data
532 are shown in Figure 1, supplement 7. Quantification of polymerization was calculated
533 using the difference between the average initial and final values of light scattering for

534 each sample (n=5 for average) in Figures 1B and 2A and supplemental figures 1S1,
535 2S1, 2S2, and 7S1. All other light scattering values are the actual values of light
536 scattering recorded (in arbitrary units), except where noted in the figure legends.
537
538 **CTP production activity assay**
539 Enzyme concentration was determined using the extinction coefficient for CtpS, 0.055
540 μM/A_{280} unit. Concentrated enzyme (40-80 μM) was annealed at room temperature for 3
541 minutes at 21˚C in10 mM $MgCl_2$, 60 mM HEPES pH 8.0, then mixed with 1.5 mM ATP
542 and 600 μM UTP and incubated 20 minutes at 37˚C. Four minute incubations with
543 substrates gave equivalent results. When CTP was present, it was included in the
544 ATP/UTP mixture. The reactions were initiated by mixing with 10 mM final glutamine and
545 the absorbance at 291 nm measured. It was not possible to measure the rates of 277R
546 above 8000 nM (19 uM/sec) because the rate could not be reliably measure considering
547 the dead time of the instrument and the procedure (~ 5 seconds). The final reactions
548 contain 0.1 - 25 mM NaCl from the enzyme storage stocks, but these concentrations of
549 NaCl do not have noticeable effects on enzyme rate. The annealing step is critical for
550 highest specific activities from stocks stored frozen or at 4˚C and is optimal at
551 concentrations greater than 2 μM. From CTP inhibition experiments, the CTP IC50 value
552 at 200 nM $CtpS^{WT}$, 600 uM UTP and 1.5 mM ATP was 360 μM (Fig. 7, supplement 2).
553 The concentration-dependences were complex and yielded curved Hill plots. IC50
554 values were obtained by linear extrapolation using points flanking v_i=1/2v_o. Graphical
555 data points represent the averaged values of 2-6 experiments with error bars indicating
556 the standard error or standard deviation of each measurement.
557
558 **CTP polymerization assay**

559 Purified CtpS protein was incubated at 37° C for 20 min in 50 mM Tris HCl (pH 7.8) and
560 10 mM $MgCl_2$. 1 mM CTP (Epicentre) was added immediately before sample was
561 loaded into the fluorometer. Time between CTP addition and initiation of sample
562 recording averaged 5 seconds. Measurements were taken as described for the
563 activity/polymerization assay.
564
565 **Ultracentrifugation activity assay**
566 Purified CtpS protein was incubated in the activity buffer or CTP buffer [1 mM CTP, 10
567 mM $MgCl_2$, 50 mM Tris-HCl (pH 7.8)] at 37° C for 1 hour. Samples were centrifuged at
568 116,000 x *g* for 15 minutes at 4° C using an Optima TLA 100 rotor (Beckman). After
569 centrifugation, the supernatant was removed. For activity assays, the pellet was
570 resuspended in 100 µl ice cold buffer containing 50 mM Tris HCL (pH 7.8) and 10 mM
571 $MgCl_2$. 10 µl of this CtpS pellet solution was added to complete activity buffer containing
572 50 mM Tris HCl (pH 7.8), 10 mM MgCl2, 1 mM UTP, 1 mM ATP, 0.2 mM GTP, and 10
573 mM glutamine to monitor initial activity.
574
575 **Quantification of native CtpS levels**
576 Wild type NCM3722 was grown to early exponential phase in M9 minimal media plus
577 0.04% glucose (M9G). Native levels of CtpS were quantified based on a standard curve
578 of purified CtpS and normalized based on the OD_{600} of the culture. Calculations assume
579 1 OD unit = 8 x 10^8 cells and cellular volume = 1 μm^3. Samples were loaded on a 10%
580 Tris-glycine SDS PAGE gel. Membrane was probed with 1:15,000 rabbit anti-CtpS.
581 Band intensities were compared using Image J.
582
583 **Quantification of CtpS in CTP buffer**

584 For quantification of CtpS pelleting in variable CTP, 130 µg CtpS was incubated in 500
585 µl appropriate concentrations of CTP buffer (4.3 µM CtpS). 200 µl samples were spun at
586 116,000 x *g* on a Beckman TLA-100 rotor for 30 minutes at 4 C. The pellet fraction was
587 resuspended in 50 ul SDS-PAGE sample buffer. Samples were loaded on a 10% Tris-
588 glycine SDS PAGE gel. Membrane was probed with 1:15,000 rabbit anti-CtpS. Band
589 intensities were compared using Image J.
590
591 **Electron microscopy**
592 *Negative stain imaging.* Negative stain EM samples were prepared by applying
593 polymerized CtpS to carbon coated grids and staining with 0.75 % uranyl formate (Ohi et
594 al., 2004). 15µM purified CTPs in 50 mM Tris HCl (pH 7.8) was incubated for 20 minutes
595 at 37˚C with 1mM CTP and 5mM $MgCl_2$, or without nucleotide as a control. Reactions
596 were diluted 1/10 in the same buffer supplemented with 50% glycerol before being
597 coated onto grids and stained with uranyl formate for analysis. Protein purifications for
598 wild-type CTPs and mutants E155K and E277R were performed simultaneously.
599 Negative stain EM was performed on a Tecnai TF20 microscope (FEI Co.) operating at
600 200 kV, and images were acquired on a 4k x 4k CCD camera (Gatan, Inc.). Micrographs
601 all taken at 55 000 X magnification.
602 *Cryo-EM imaging.* 15µM purified CTPs was incubated for 20 min. at 37˚C in activity
603 buffer. Samples were prepared by applying polymerized CtpS to glow-discharged
604 Quantifoil holey-carbon grids (Quantifoil Micro Tools GmbH), blotting in a Vitrobot (FEI
605 Co.) and rapidly plunging into liquid ethane. Cryo-EM data were obtained on a Titan
606 Krios operating at 200 kV with a 4k x 4k Gatan Ultrascan camera at a pixel size of 0.82
607 Å /pixel. Total electron dose was in the range of 25-30 e-/A^2 per image, and images
608 were acquired over a defocus range of -1 to -3.5 µm (average -2.5 µm).
609

610 **Image processing**

611 Defocus parameters for each micrograph were determined with CTFFIND (Mindell and
612 Grigorieff, 2003). CTF correction was achieved by applying a Wiener filter to the entire
613 micrograph. Lengths of helix were defined in the boxer program of the EMAN software
614 suite (Ludtke et al., 1999). Overlapping segments were extracted from the CTF-
615 corrected micrographs along the length of each helix. In total, 12,465 overlapping
616 segments were extracted in 510 x 510 Å boxes, representing approximately 56,000
617 unique CtpS monomers. Segments were binned twofold prior to reconstruction, at a
618 final pixel size of 1.64 Å. Iterative helical real space reconstruction (IHRSR) was
619 performed essentially as described by Egelman and Sasche, et al (Egelman, 2007;
620 Sachse et al., 2007), using SPIDER (Frank, 1996) for projection matching and back
621 projection, and hsearch_lorentz (Egelman, 2000) for refinement of helical symmetry
622 parameters. A cylinder was used as the initial reference volume, and thirty rounds of
623 iterative refinement were carried out at increasingly smaller angular increments (1.5° in
624 the final round). A preliminary reconstruction was performed imposing only helical
625 symmetry, from which it was clear that the repeating helical subunit was the CtpS
626 tetramer; in subsequent runs of IHRSR the local 2-2-2 point group symmetry of the CtpS
627 tetramer was also enforced. Visualization of the cryo-EM reconstructions and rigid body
628 fitting of the CtpS crystal structure into the EM map were performed in Chimera
629 (Pettersen et al., 2004). The CtpS crystal structure monomer was initially fit as a single
630 rigid body into the EM map, followed by local refinement of the fit treating the two
631 domains and linker region as three separate rigid bodies. The final EM map was
632 amplitude corrected using amplitudes from the atomic model.

633

634 **Site-directed mutagenesis**

635 Site-directed mutagenesis was performed using the QuickChange (Agilent) system with
636 minor modifications to enable using KOD polymerase (Millipore) or GXL polymerase
637 (Takara).
638
639 **Live cell imaging**
640 Strains were grown overnight in LB with 50 ug/ml carbenicillin, subcultured and grown
641 until early exponential phase. Fluorescent protein expression was induced with 0.01 mM
642 IPTG for 2-3 hours. Cells were immobilized on 1% agarose in water pads containing
643 0.01 mM IPTG. Imaging was performed using a Nikon TI-E microscope using a 100X
644 Nikon Plan Apo objective (NA = 1.4), Chroma ET572/35X (excitation) and ET622/60M
645 (emission), Prior Lumen 200 Pro illumination, and 89014VS dichroic mirro. Images were
646 acquired with an Andor Clara camera using NIS-Elements software.
647
648 **Chromosomal integration of CtpS^{E277R}**
649 PCR fragments of the region from *mazG* to *ygcG* either containing a wild type *pyrG* or
650 *pyrG*^{E277R} coding region and a kanamycin resistance cassette between *eno* and *ygcG*
651 were integrated into the NCM3722 chromosome by Lamda red recombination.
652 Recombineered cells were recovered on LB agar with 50 ug/ml kanamycin and 200
653 ug/ml cytidine.
654
655 **Growth curves**
656 Strains were grown overnight in LB containing 30 µg/ml kanamycin and 200 µg/ml
657 cytidine. Then cells were diluted to the same OD in 100 µl LB plus kanamycin or M9G
658 plus kanamycin (as noted) in a 96 well format. OD_{600} was recorded using a BioTek
659 microplate reader at 37°C with continuous shaking.
660

661 **Metabolomics of CtpS^{E277R} chromosomal integrant**

662 Strains were grown in M9 minimal media to early exponential phase. Media was
663 supplemented with 13C5-ribose labeled cytidine (Cambridge Isotopes) to a final
664 concentration of 200 ug/ml and cell growth was continued at 37°C. Sample preparations
665 was modified based on Lu *et al* (Lu et al., 2007). Specifically, 24 milliliters of bacterial
666 cultures were harvested by centrifugation at room temperature at five time points
667 following cytidine addition: 0 minute, 5 minutes, 20 minutes, 60 minutes, and 120
668 minutes. The pellet was resuspended in 1 ml 40:40:20 methanol:acetonitrile:water
669 quenching buffer and allowed to sit on dry ice for 15 min. Sample was spun at maximum
670 speed in a microcentrifuge for 5 min at 4°C. Then the resulting pellet was resuspended
671 again in 0.6 ml fresh 40:40:20 solution for 15 min on dry ice and then spun as before to
672 quench and extract metabolites a second time. Quenching buffer supernatants were
673 combined and concentrated three-fold for mass spectrometry as in Xu *et al (Xu et al.,*
674 *2012).*
675

Acknowledgements

We acknowledge the members of the Gitai lab, in particular E. Klein, A. Siryaporn, R. Morgenstein, and M. Wilson, for helpful discussions and N. Ouzounov for assistance in strain construction. In addition to the Rabinowitz lab, we specifically thank W. Lu and J. Rabinowitz for advice and J. Fan for assistance with metabolic profiling. Crl antibodies were a gift of the Silhavy lab. We are grateful to the Facility for Electron Microscopy Research at McGill University for use of electron microscopes and for staff assistance. We would like to thank M. Shepherd for assistance in image processing.

Accession Numbers

The cryo-EM map of the CtpS filament has been deposited with the Electron Microscopy Data Bank [EMDB] accession number EMD-2700.

Financial Disclosure

J.K. and Z.G. are supported by a Human Frontier Science Program Award. Z.G. is supported by an NIH New Innovator Award (1DP2OD001491) and NIH Grant (5RO1GM107384). A.F.B. acknowledges the support of the Human Frontier Science Program, as well as partial support by National Science Foundation Grant PHY-0957573 and National Institutes of Health Grant R01 GM082938. The funders had no role in study design, data collection and analysis, decision to publish, or preparation of the manuscript.

Author Contributions

R.M.B., A.L., E.J.C., H.L., C.H., J.H., and J.K. performed experiments and analyzed data. A.F.B. and N.S.W. designed and performed mathematical modeling. R.M.B.,

E.P.B., J.K., and Z.G. designed experiments. R.M.B., A.F.B., J.K., and Z.G. wrote the paper.

705 **References:**

706 Anderson, P.M. (1983). CTP synthetase from *Escherichia coli*: an improved purification
707 procedure and characterization of hysteretic and enzyme concentration effects on kinetic
708 properties. Biochemistry *22*, 3285-3292.

709 Ayengar, P., Gibson, D.M., and Sanadi, D.R. (1956). Transphosphorylations between
710 nucleoside phosphates. Biochim Biophys Acta *21*, 86-91.

711 Barry, R.M., and Gitai, Z. (2011). Self-assembling enzymes and the origins of the
712 cytoskeleton. Curr Opin Microbiol *14*, 704-711.

713 Carcamo, W.C., Calise, S.J., von Muhlen, C.A., Satoh, M., and Chan, E.K. (2014).
714 Molecular cell biology and immunobiology of mammalian rod/ring structures. Int Rev Cell
715 Mol Biol *308*, 35-74.

716 Chakraborty, K.P., and Hurlbert, R.B. (1961). Role of glutamine in the biosynthesis of
717 cytidine nucleotides in *Escherichia coli*. Biochim Biophys Acta *47*, 607-609.

718 Chen, K., Zhang, J., Tastan, O.Y., Deussen, Z.A., Siswick, M.Y., and Liu, J.L. (2011).
719 Glutamine analogs promote cytoophidium assembly in human and *Drosophila* cells. J
720 Genet Genomics *38*, 391-402.

721 Egelman, E.H. (2000). A robust algorithm for the reconstruction of helical filaments using
722 single-particle methods. Ultramicroscopy *85*, 225-234.

723 Egelman, E.H. (2007). The iterative helical real space reconstruction method:
724 surmounting the problems posed by real polymers. J Struct Biol *157*, 83-94.

725 Endrizzi, J.A., Kim, H., Anderson, P.M., and Baldwin, E.P. (2004). Crystal structure of
726 *Escherichia coli* cytidine triphosphate synthetase, a nucleotide-regulated glutamine
727 amidotransferase/ATP-dependent amidoligase fusion protein and homologue of
728 anticancer and antiparasitic drug targets. Biochemistry *43*, 6447-6463.

729 Endrizzi, J.A., Kim, H., Anderson, P.M., and Baldwin, E.P. (2005). Mechanisms of
730 product feedback regulation and drug resistance in cytidine triphosphate synthetases
731 from the structure of a CTP-inhibited complex. Biochemistry *44*, 13491-13499.
732 Forbes, S.A., Bhamra, G., Bamford, S., Dawson, E., Kok, C., Clements, J., Menzies, A.,
733 Teague, J.W., Futreal, P.A., and Stratton, M.R. (2008). The Catalogue of Somatic
734 Mutations in Cancer (COSMIC). Curr Protoc Hum Genet *Chapter 10*, Unit 10 11.
735 Frank, J. (1996). Three-Dimensional Electron Microscopy of Macromolecular Assemblies
736 (San Diego, Academic Press, Inc.).
737 Fricke, J., Neuhard, J., Kelln, R.A., and Pedersen, S. (1995). The cmk gene encoding
738 cytidine monophosphate kinase is located in the rpsA operon and is required for normal
739 replication rate in Escherichia coli. J Bacteriol *177*, 517-523.
740 Goto, M., Omi, R., Nakagawa, N., Miyahara, I., and Hirotsu, K. (2004). Crystal structures
741 of CTP synthetase reveal ATP, UTP, and glutamine binding sites. Structure *12*, 1413-
742 1423.
743 Gou, K.M., Chang, C.C., Shen, Q.J., Sung, L.Y., and Liu, J.L. (2014). CTP synthase
744 forms cytoophidia in the cytoplasm and nucleus. Exp Cell Res *323*, 242-253.
745 Hofer, A., Steverding, D., Chabes, A., Brun, R., and Thelander, L. (2001). *Trypanosoma*
746 *brucei* CTP synthetase: a target for the treatment of African sleeping sickness. Proc Natl
747 Acad Sci U S A *98*, 6412-6416.
748 Holm, L., and Sander, C. (1993). Protein structure comparison by alignment of distance
749 matrices. J Mol Biol *233*, 123-138.
750 Ingerson-Mahar, M., Briegel, A., Werner, J.N., Jensen, G.J., and Gitai, Z. (2010). The
751 metabolic enzyme CTP synthase forms cytoskeletal filaments. Nat Cell Biol *12*, 739-746.
752 Jackson-Fisher, A.J., Burma, S., Portnoy, M., Schneeweis, L.A., Coleman, R.A., Mitra,
753 M., Chitikila, C., and Pugh, B.F. (1999). Dimer dissociation and thermosensitivity kinetics

754 of the Saccharomyces cerevisiae and human TATA binding proteins. Biochemistry *38*,
755 11340-11348.
756 Levitzki, A., and Koshland, D.E., Jr. (1972a). Ligand-induced dimer-to-tetramer
757 transformation in cytosine triphosphate synthetase. Biochemistry *11*, 247-253.
758 Levitzki, A., and Koshland, D.E., Jr. (1972b). Role of an allosteric effector. Guanosine
759 triphosphate activation in cytosine triphosphate synthetase. Biochemistry *11*, 241-246.
760 Liu, J.L. (2010). Intracellular compartmentation of CTP synthase in Drosophila. J Genet
761 Genomics *37*, 281-296.
762 Long, C.W., and Pardee, A.B. (1967). Cytidine triphosphate synthetase of *Escherichia*
763 *coli* B. I. Purification and kinetics. J Biol Chem *242*, 4715-4721.
764 Lu, W., Kwon, Y.K., and Rabinowitz, J.D. (2007). Isotope ratio-based profiling of
765 microbial folates. J Am Soc Mass Spectrom *18*, 898-909.
766 Ludtke, S.J., Baldwin, P.R., and Chiu, W. (1999). EMAN: semiautomated software for
767 high-resolution single-particle reconstructions. J Struct Biol *128*, 82-97.
768 Meng, Q., Turnbough, C.L., Jr., and Switzer, R.L. (2004). Attenuation control of pyrG
769 expression in *Bacillus subtilis* is mediated by CTP-sensitive reiterative transcription. Proc
770 Natl Acad Sci U S A *101*, 10943-10948.
771 Michaelis, A.M., and Gitai, Z. (2010). Dynamic polar sequestration of excess MurG may
772 regulate enzymatic function. J Bacteriol *192*, 4597-4605.
773 Mindell, J.A., and Grigorieff, N. (2003). Accurate determination of local defocus and
774 specimen tilt in electron microscopy. J Struct Biol *142*, 334-347.
775 Miraldi, E.R., Thomas, P.J., and Romberg, L. (2008). Allosteric models for cooperative
776 polymerization of linear polymers. Biophys J *95*, 2470-2486.
777 Noree, C., Sato, B.K., Broyer, R.M., and Wilhelm, J.E. (2010). Identification of novel
778 filament-forming proteins in *Saccharomyces cerevisiae* and *Drosophila melanogaster*. J
779 Cell Biol *190*, 541-551.

780 Ohi, M., Li, Y., Cheng, Y., and Walz, T. (2004). Negative Staining and Image
781 Classification - Powerful Tools in Modern Electron Microscopy. Biological procedures
782 online *6*, 23-34.
783 Ostrander, D.B., O'Brien, D.J., Gorman, J.A., and Carman, G.M. (1998). Effect of CTP
784 synthetase regulation by CTP on phospholipid synthesis in *Saccharomyces cerevisiae*. J
785 Biol Chem *273*, 18992-19001.
786 Pappas, A., Yang, W.L., Park, T.S., and Carman, G.M. (1998). Nucleotide-dependent
787 tetramerization of CTP synthetase from *Saccharomyces cerevisiae*. J Biol Chem *273*,
788 15954-15960.
789 Perutz, M.F. (1989). Mechanisms of cooperativity and allosteric regulation in proteins. Q
790 Rev Biophys *22*, 139-237.
791 Pettersen, E.F., Goddard, T.D., Huang, C.C., Couch, G.S., Greenblatt, D.M., Meng,
792 E.C., and Ferrin, T.E. (2004). UCSF Chimera--a visualization system for exploratory
793 research and analysis. J Comput Chem *25*, 1605-1612.
794 Sachse, C., Chen, J.Z., Coureux, P.D., Stroupe, M.E., Fandrich, M., and Grigorieff, N.
795 (2007). High-resolution electron microscopy of helical specimens: a fresh look at tobacco
796 mosaic virus. J Mol Biol *371*, 812-835.
797 Soupene, E., van Heeswijk, W.C., Plumbridge, J., Stewart, V., Bertenthal, D., Lee, H.,
798 Prasad, G., Paliy, O., Charernnoppakul, P., and Kustu, S. (2003). Physiological studies
799 of Escherichia coli strain MG1655: growth defects and apparent cross-regulation of gene
800 expression. J Bacteriol *185*, 5611-5626.
801 Trudel, M., Van Genechten, T., and Meuth, M. (1984). Biochemical characterization of
802 the hamster thy mutator gene and its revertants. J Biol Chem *259*, 2355-2359.
803 Valentin-Hansen, P. (1978). Uridine-cytidine kinase from Escherichia coli. Methods
804 Enzymol *51*, 308-314.

805 van den Ent, F., Amos, L.A., and Lowe, J. (2001). Prokaryotic origin of the actin
806 cytoskeleton. Nature *413*, 39-44.
807 Williams, J.C., Kizaki, H., Weber, G., and Morris, H.P. (1978). Increased CTP synthetase
808 activity in cancer cells. Nature *271*, 71-73.
809 Xu, Y.-F., Zhao, X., Glass, D.S., Absalan, F., Perlman, D.H., Broach, J.R., and
810 Rabinowitz, J.D. (2012). Regulation of Yeast Pyruvate Kinase by Ultrasensitive Allostery
811 Independent of Phosphorylation. Molecular Cell *48*, 52-62.
812 Yang, W.L., Bruno, M.E., and Carman, G.M. (1996). Regulation of yeast CTP synthetase
813 activity by protein kinase C. J Biol Chem *271*, 11113-11119.
814
815
816
817

818
819 **Figure Legends**

820 **Figure 1. CtpS polymerization and enzymatic activity are inversely related. (A)** A
821 model of oligomeric regulation of CtpS. Tetramer formation from CtpS dimers is favored
822 by a combination of enzyme concentration as well as nucleotide (substrates ATP and
823 UTP or product CTP) and Mg^{2+} binding. **(B)** CtpS was incubated in activity buffer
824 containing all substrates for CTP production. As the enzyme concentration increases,
825 CtpS shows assembly by light scattering and the k_{cat} value (V_{obs}/[CtpS]) decreases. Error
826 bars = standard error (SE), n=3-5. **(C)** Negative stain image of CtpS filaments
827 assembled after CTP synthesis reaction. Smaller particles in the background resemble
828 the X-shaped CtpS tetramer. A single filament is shown at bottom. **(D)** CtpS polymers
829 formed in activity buffer were ultracentrifuged to pellet polymers. The pellet fraction was
830 resuspended and CTP production recorded. **(E)** CtpS assembly and activity were
831 assayed after CtpS was first polymerized, followed by addition of saturating amounts of
832 substrate after 600 seconds.
833

834 **Figure 2. CTP is sufficient and necessary to stimulate CtpS polymerization. (A)**
835 CtpS levels were titrated in buffer containing 1mM CTP (with no substrates present).
836 Polymerization was observed in the same range of protein concentrations as in activity
837 buffer. Error bars = SE, n=3. **(B)** CtpS was allowed to polymerize at different CTP
838 concentrations (with no substrates present). The polymers were collected by
839 ultracentrifugation and changes in CtpS pellet abundance were quantified by
840 immunoblot. Error bars = SE, n=2. **(C)** Purified $CtpS^{E155K}$, which is defective in CTP
841 binding, showed no obvious changes in light scattering during the normal conditions of
842 wild-type polymer assembly in activity buffer. Initial light scattering values were
843 normalized to 1 to place wild type CtpS and $CtpS^{E155K}$ on the same scale. Error bars =

844 SE, n=3. **(D)** CtpS Filaments of wild-type and mutants by negative stain electron
845 microscopy. There were very few filaments observed in the absence of CTP (top row).
846 Upon the addition of nucleotide and $MgCl_2$, filaments were only observed in the wild-type
847 sample (first column). Micrographs were all taken at 55,000 X magnification. **(E)** CtpS
848 was incubated in the inhibitor DON and 1 mM CTP and allowed to polymerize. Addition
849 of ATP and UTP depolymerized the sample. Polymers did not reform.
850
851 **Figure 3. Cryo-EM structure of CtpS filaments at 8.4 Å resolution. (A)** A segment of
852 the reconstructed filament, colored by helical subunit. **(B)** The *E. coli* CtpS crystal
853 structure monomer fit into the cryo-EM density. Each domain was fit as a separate rigid
854 body. **(C)** Novel filament assembly contacts between the linker domains. **(D)** Novel
855 assembly contacts between the GATase domains.
856
857 **Figure 4. Rearrangement of the CtpS tetramerization interface within the filament.**
858 **(A)** Superposition of the *E. coli* crystallographic tetramer (grey) with the atomic model
859 from the cryo-EM structure (color), shows a rearrangement of the tetramerization
860 contacts, primarily a compression of the tetramer along the filament axis. **(B)**
861 Rearrangements of the tetramerization contacts shift the relative positions of helices
862 near bound CTP (grey: crystal structure; color cryo-EM structure).
863
864 **Figure 5. Implications of the CtpS filament structure for the mechanism of enzyme**
865 **inhibition. (A)** The binding sites for ATP, CTP, and glutamine are all solvent accessible
866 in the filament, suggesting that they are freely exchangeable in the filament form. **(B)**
867 The approximate direction of the putative rotation of the glutaminase domain toward the
868 amidoligase domain (arrow), which is predicted to create a shorter channel for ammonia

869 diffusion. **(C)** In the filament structure, such a conformational change would be sterically
870 hindered by contacts with adjacent filament subunits.
871
872 **Figure 6. Linker helix residues form a polymerization interface. (A)** The positions of
873 the four polymerization mutants in the model of the linker-linker filament assembly
874 interface. **(B)** Point mutants were engineered into an mCherry-CtpS fusion and imaged
875 upon expression in *E. coli*. Scale bar = 3 microns. Wild type mCherry-CtpS forms
876 filaments while mutant mCherry-CtpSs show diffuse localizations.
877
878 **Figure 7. Linker helix mutations disrupt polymerization and cause a growth defect.**
879 **(A)** The CTP production activity of titrated levels of $CtpS^{E227R}$ exhibited a small decrease
880 in enzymatic activity as enzyme concentration increases when compared to wild type
881 protein. Error bars = SD n=3-6). **(B)** Purified $CtpS^{E277R}$ does not polymerize in the
882 presence of CTP. For both wild type and E277R CtpS there were very few filaments
883 observed in the absence of CTP (top row). Upon the addition of nucleotide and $MgCl_2$,
884 filaments were only observed in the wild-type sample (first column). **(C)** Growth curve
885 comparing wild type and $CtpS^{E277R}$ cells in LB media. $CtpS^{E277R}$ exhibits defective growth
886 when compared to cells with wild type CtpS. Both strains were grown overnight and
887 subcultured into LB media. Growth curve comparing wild type to the defective growth of
888 $CtpS^{E277R}$ mutant *E. coli* in minimal media. $CtpS^{E277R}$ mutants exhibit defective growth.
889 Error bars = SE, n=18.
890
891 **Figure 8. Mutation of polymerization interface disrupts CTP homeostasis *in vivo*.**
892 **(A)** Metabolic profiling of wild type and $CtpS^{E277R}$ mutant cells after addition of cytidine to
893 minimal media. Nucleotide biosynthesis molecules are shown. **(B)** Incorporation of C13-
894 label into CTP pool in wild type and $CtpS^{E277R}$ mutant cells. Incorporation occurs at

895 similar levels in both strains. Error bars = SE, n=3. **(C)** The proportion of unlabeled
896 (C12) CTP in wild type and CtpS^{E277R} mutant cells. The ratio of C12-CTP to total CTP is
897 higher in the CtpS^{E277R} strain. Error bars = SE, n=3. **(D)** Model of the fraction of active
898 (nonpolymerized and UTP-bound) CtpS, plotted versus CTP concentration. Comparison
899 is shown between competitive inhibition with polymerization, noncompetitive inhibition
900 with polymerization, competitive-nonpolymerizing, and noncompetitive-nonpolymerizing
901 mechanisms. In all cases, we chose a fixed UTP concentration equal to K_{cp}, the
902 dissociation constant of CTP and polymerized CtpS (see Supplementary Material for
903 details).
904
905 **Figure 9. An expanded description of CtpS assembly.** As shown in Fig. 1A, tetramer
906 formation from CtpS dimers is favored by a combination of enzyme concentration as well
907 as nucleotide (substrates ATP and UTP or product CTP) and Mg^{2+} binding. CTP binding
908 and higher enzyme concentration further stimulates reversible formation of inhibited
909 polymeric filaments, which can be disassembled by ATP/UTP.
910
911

912 **Figure Supplement:**

913 **Figure 1, supplement 1. Determination of threshold concentration for CtpS**
914 **polymerization in activity buffer. (A)** Below 1 μM, the changes in light scattering (blue)
915 are very low. At low [CtpS] the net changes in light scattering were both above and
916 below zero, so the absolute values are plotted to allow comparison on a logarithmic plot
917 (only the values for 0.05 μM and 0.075 μM CtpS were above zero). CtpS activity (red) is
918 plotted on a logarithmic plot to compare the concentration at which polymerization and
919 activity decreases begin. **(B)** The logarithmic plot of polymerization shows an inflection
920 point at 1 μM. This predicts an approximate threshold concentration for polymerization
921 between 1 μM and 2 μM.

922

923 **Figure 1, supplement 2. Representative examples of raw data from three different**
924 **concentrations of CtpS incubated in activity buffer included in Figure 1B.** Light
925 scattering (polymerization) is shown in blue and transmittance data (CTP accumulation)
926 is shown in red. **(A)** 100 nM CtpS (below polymerization threshold). **(B)** 2 uM CtpS (at
927 polymerization threshold). **(C)** 5 uM CtpS (above polymerization threshold).

928

929 **Figure 1, supplement 3. Calculation of intracellular CtpS in minimal media.** Levels
930 of native CtpS protein in wild type *E. coli* NCM3722 were compared to dilutions of the
931 purified protein of known concentration (9 mg/ml). Band intensities were quantified using
932 Image J. Amount of cells in lysate was approximated to be $8x10^8/OD_{600}$ unit. Volume of
933 an *E. coli* cell was approximated to be 1 um^3.

934

935 **Figure 1, supplement 4. CtpS activity is not sensitive to incubation on ice.** Due to
936 concerns that placing resuspended polymers on ice may affect enzymatic activity
937 significantly, we compared the activity level of CtpS reactions under typical conditions

938 (t=0 min) versus incubation on ice. For later time points, 10 µl of cold CtpS-containing
939 buffer was added to room temperature activity buffer to match the conditions of the
940 ultracentrifuguation assay (Fig. 1C). Overall activity does not change over the course of
941 the experiment at the lower temperature.
942
943 **Figure 1, supplement 5. CtpS higher order structures disassemble over time after**
944 **centrifugation.** Light scattering values from the pellet fraction of polymerized CtpS
945 decrease over time after centrifugation from a baseline initial value. Pellet fraction
946 stored on ice and compared to initial light scattering value immediately after
947 resuspension.
948
949 **Figure 1, supplement 6. CtpS polymer disassembly is not cause by mechanical**
950 **disruption of polymers.** Addition of an equivalent volume of water to the volume
951 contributed by substrates added in Fig. 1E to polymerized CtpS does not change light
952 scattering values. Error bars in B are the standard deviation of light scattering values
953 over the time course shown in A.
954
955 **Figure 1, supplement 7. Correction of k_{cat} values between initial Princeton and UC**
956 **Davis data sets.** Linear correction was performed as described in Methods to generate
957 overlapping data sets.
958
959 **Figure 2, supplement 1. CtpS enzymatic activity or CTP addition is required for**
960 **CtpS polymerization.** Addition of various factors (shown in table) to 10 µM CtpS
961 indicates that glutamine binding is dispensable for CtpS polymerization. Full activity
962 buffer (containing 1 mM ATP, 1 mM UTP, and 10 mM glutamine) or CTP are required for
963 polymerization. Omission of a substrate from activity buffer or addition of the inhibitor 1

964 mM DON inhibits polymerization. 1 mM DON has no effect on CTP-induced

965 polymerization. Error bars = SE (n=2).

966 **Figure 2, supplement 2. Determination of threshold concentration for CtpS**
967 **polymerization in 1 mM CTP.** Threshold concentration was calculated as in Fig. 1,
968 supplement 1 for CtpS incubated in buffer with 1 mM CTP. The graph shows an
969 inflection point at 1-2 μM. Error bars = SE (n=3).
970
971 **Figure 2, supplement 3. Immunoblot of CtpS pelleted by ultracentrifugation.** CtpS
972 was incubated in titrating amounts of CTP as described in Methods. Pellet fraction band
973 density was calculated by ImageJ to determine fold change.
974
975 **Figure 2, supplement 4. DON-treated CtpS is enzymatically inactive.** Samples of
976 CtpS were allowed to polymerize in activity buffer. Then 10 mM DON was added to stop
977 enzymatic activity. **(A,B)** Two independent representative experiments are shown. Light
978 scattering (polymerization) and transmittance (CTP production) are shown on the same
979 axis in arbitrary units. **(C)** Polymerization and activity before and after DON addition are
980 compared. Overall amplitude of light scattering and transmittance data is affected by
981 absorption by DON at the wavelengths of light used for the assay. Therefore, the slopes
982 of each condition are shown.
983
984 **Figure 2, supplement 5. DON inhibition of activity does not inhibit polymerization**
985 **upon CTP addition.** In the converse experiment of Figure 2E, DON-inhibited CtpS
986 incubated in substrates does not polymerize, but addition of 1 mM CTP stimulates
987 polymerization.
988
989 **Figure 3, supplement 1. Cryo-EM reconstruction of CtpS filaments. (A)** A field of
990 CtpS filaments in cryo-EM. **(B)** Cryo-EM image of a single CtpS filament. **(C)** The
991 reconstruction of CtpS filament shown at 8.4 Å resolution. In addition to the refined

992 helical symmetry, local 2-2-2 point group symmetry was imposed on each helical
993 subunit. **(D)** The resolution of the final reconstruction was estimated in two ways: the
994 standard even-odd half volume test (blue), and a comparison of the cryo-EM structure to
995 the atomic model (red). For both measures, the resolution is estimated at 10.4 Å by the
996 0.5 cutoff criterion, and 8.4 Å by the 0.143 criterion.
997
998 **Figure 3, supplement 2. The CtpS monomer in the filament is in a similar**
999 **conformation to crystallographic structures, and ADP and CTP are present. (A)**
1000 The fit CtpS monomer structure (orange) is overlaid with the available crystal structures
1001 of full-length CtpS (grey), aligned on the N-terminal ALase domain. **(B)** A difference map
1002 (blue mesh) was calculated between a model of the CtpS filament calculated from the fit
1003 crystal structure and the EM structure. Strong density (here rendered at 8 σ) is
1004 observed for CTP in its binding site, while the ALase active site (red residues) remains
1005 empty. **(C)** Similarly strong density is found in the difference map in the positions of
1006 bound ADP. **(D)** Very weak density is observed for glutamine in the glutaminase active
1007 site (orange sticks), and no density associated with the proposed GTP binding site (red),
1008 suggesting weak or no binding of glutamine or GTP.
1009
1010 **Figure 6, supplement 1. Sequence alignment of several CtpS primary sequences.**
1011 Note that the linker region is comprised of residues 274 – 284 in the *E. coli* sequence.
1012 The primary sequence of this region is not strongly conserved across species, however,
1013 there are several potential electrostatic (blue, purple) or hydrophobic (red) pi-stacking
1014 interactions between residues of adjacent tetramers. The linker region and nearby
1015 residues where site-mutations were engineered into *E. coli* CtpS is boxed in black.
1016
1017

1018 **Figure 7, supplement 1. CtpS^{E277R} does not polymerize *in vitro*.** Right angle light
1019 scattering by CtpS^{E277R} in activity buffer. Error bars = SE, n=3.
1020
1021 **Figure 7, supplement 2. Polymerization enhances the inhibition of CtpS activity**
1022 **by CTP.** At a CtpS concentration below the threshold concentration, (200 nM, *red*
1023 *circles*), the CTP IC50 value is 330 M. At concentrations that favor polymerization (4
1024 M CtpS, *green squares*), CTP binds with higher apparent affinity with an IC50 of 170
1025 M. Abolishing polymerization with E277R mutation reduced apparent CTP activity
1026 inhibtion (IC50=833 M at 200 nM CtpS^{E277R}) (*purple open diamonds*). The CTP
1027 synthesis v_o values before normalization were 1.24, 18.5 and 0.82 M/sec for 200 nM
1028 CtpS, 4 M CtpS and 200 nM CtpS^{E277R}, respectively.
1029
1030 **Figure 7, supplement 3. Growth curve comparing wild type to the defective growth**
1031 **of CtpS^{E277R} mutant *E. coli* in minimal media.** CtpS^{E277R} mutants exhibit defective
1032 growth. Error bars = SE, n=36.
1033
1034 **Figure 7, supplement 4. CtpS protein levels are not depleted in the CtpS^{E277R}**
1035 **mutant. (A)** Immunoblot probing CtpS and Crl (loading control) levels in NCM3722 kan^R
1036 and CtpS^{E277R} cells after the addition of 200 µg/ml. **(B)** Relative intensity of CtpS
1037 normalized to Crl levels.
1038
1039 **Figure 8, supplement 1. Metabolomic analysis of wild type and CtpS^{E277R} *E. coli***
1040 **after addition of 200 µg/ml C13-cytidine.** Fold changes of metabolite levels of
1041 NCM3722 kan^R *E. coli* and CtpS^{E277R} *E. coli* were compared to wild type levels at 0
1042 minutes. Hierarchical clustering of metabolites is shown.

1043 **Figure 8, supplement 2. CTP levels probed by mass spectrometry after addition of**
1044 **C13-labeled cytidine to the media.** Unlabeled C12-CTP population represents the
1045 proportion of CTP synthesized by CtpS from cellular pools of UTP. The $CtpS^{E277R}$ has a
1046 higher intracellular C12-CTP pool both at the initial time point as well as at the end of the
1047 time course, where C12-CTP is almost twice as high as in the wild type strain.
1048
1049 **Figure 8, supplement 3. CTP binding enhances polymerization with a sharp**
1050 **response.** The concentration required to reduce CtpS specific activity (k_{cat}) to 50% of its
1051 maximum value, $[CtpS]_{0.5}$, is inversely related to the affinity of the polymer for Ctps
1052 tetramers. In the absence of CTP, the $[CtpS]_{0.5}$ value is 3.3 □M (*red circles*). At a CTP
1053 concentration near the IC50 value (400 □M), the $[CtpS]_{0.5}$ value is slightly reduced (2.8
1054 □M, *green squares*), while at 800 □M, the $[CtpS]_{0.5}$ value significantly shifted towards
1055 polymerization ($[CtpS]_{0.5}$=1.4 □M, *blue open diamonds*). The maximum k_{cat} values before
1056 normalization were 6.7, 3.5, and 1.04 sec^{-1} for experiments using 0, 400 and 800 □M
1057 CTP, respectively.
1058

1059 **Supplementary File 1. Model of CtpS polymerization and inhibition.**

1060

1061

1062

1063

1064

1065

1066
1067

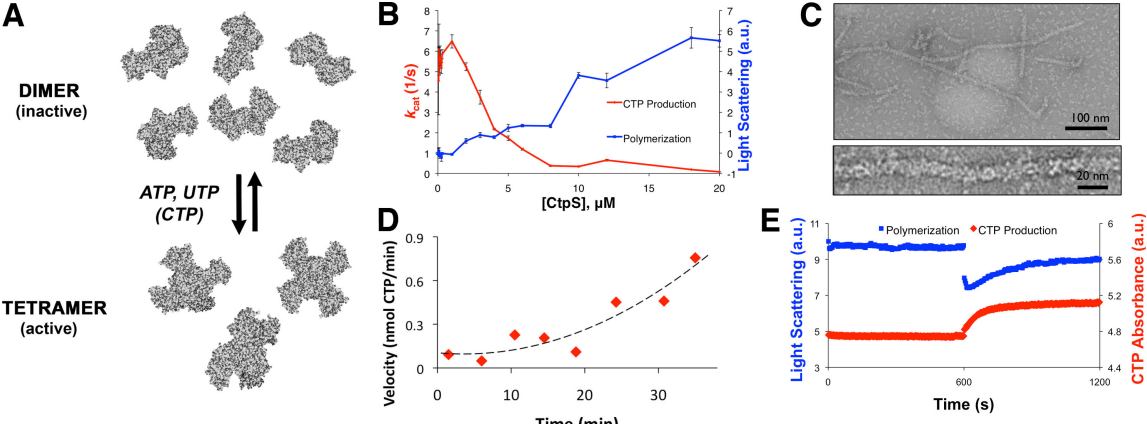
A
DIMER
(inactive)
ATP, UTP
(CTP)
TETRAMER
(active)
B
k_{cat} (1/s)
Light Scattering (a.u.)
CTP Production
Polymerization
[CtpS], μM
C
100 nm
20 nm
D
Velocity (nmol CTP/min)
Time (min)
E
Polymerization
CTP Production
Light Scattering (a.u.)
CTP Absorbance (a.u.)
Time (s)

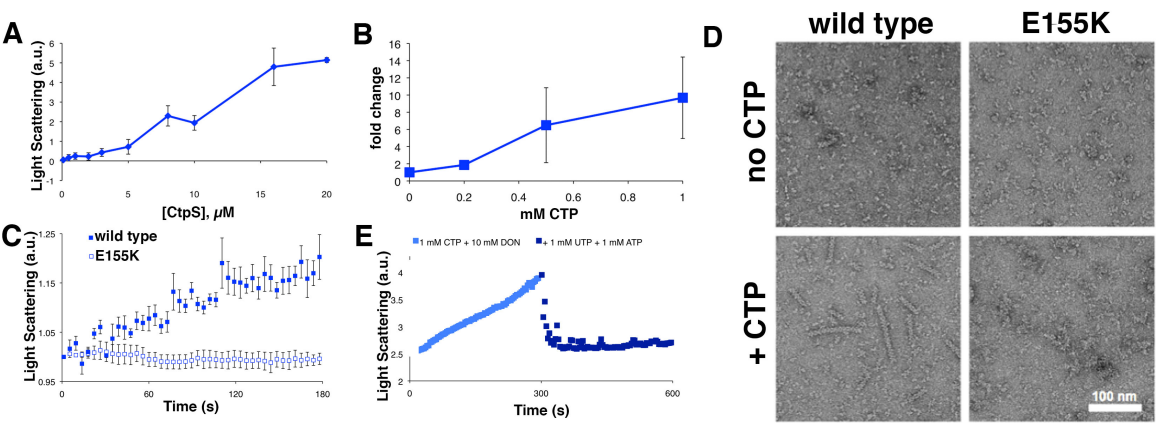
A
Light Scattering (a.u.)
[CtpS], μM
B
fold change
mM CTP
C
wild type
E155K
Light Scattering (a.u.)
Time (s)
E
1 mM CTP + 10 mM DON
+ 1 mM UTP + 1 mM ATP
Light Scattering (a.u.)
Time (s)
D
wild type
E155K
no CTP
+ CTP
100 nm

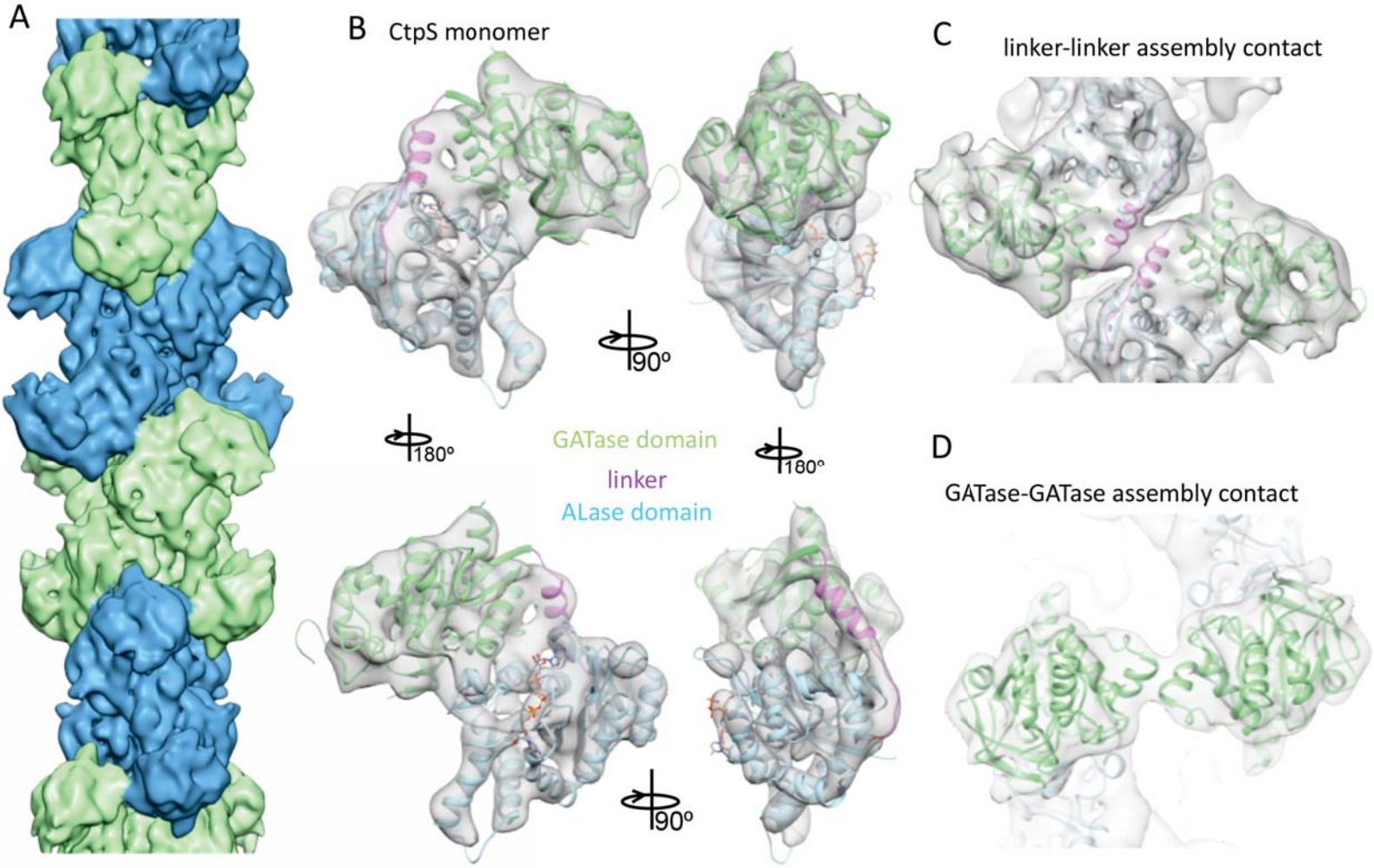
A
B
CtpS monomer
90°
180°
GATase domain
linker
ALase domain
180°
90°
C
linker-linker assembly contact
D
GATase-GATase assembly contact

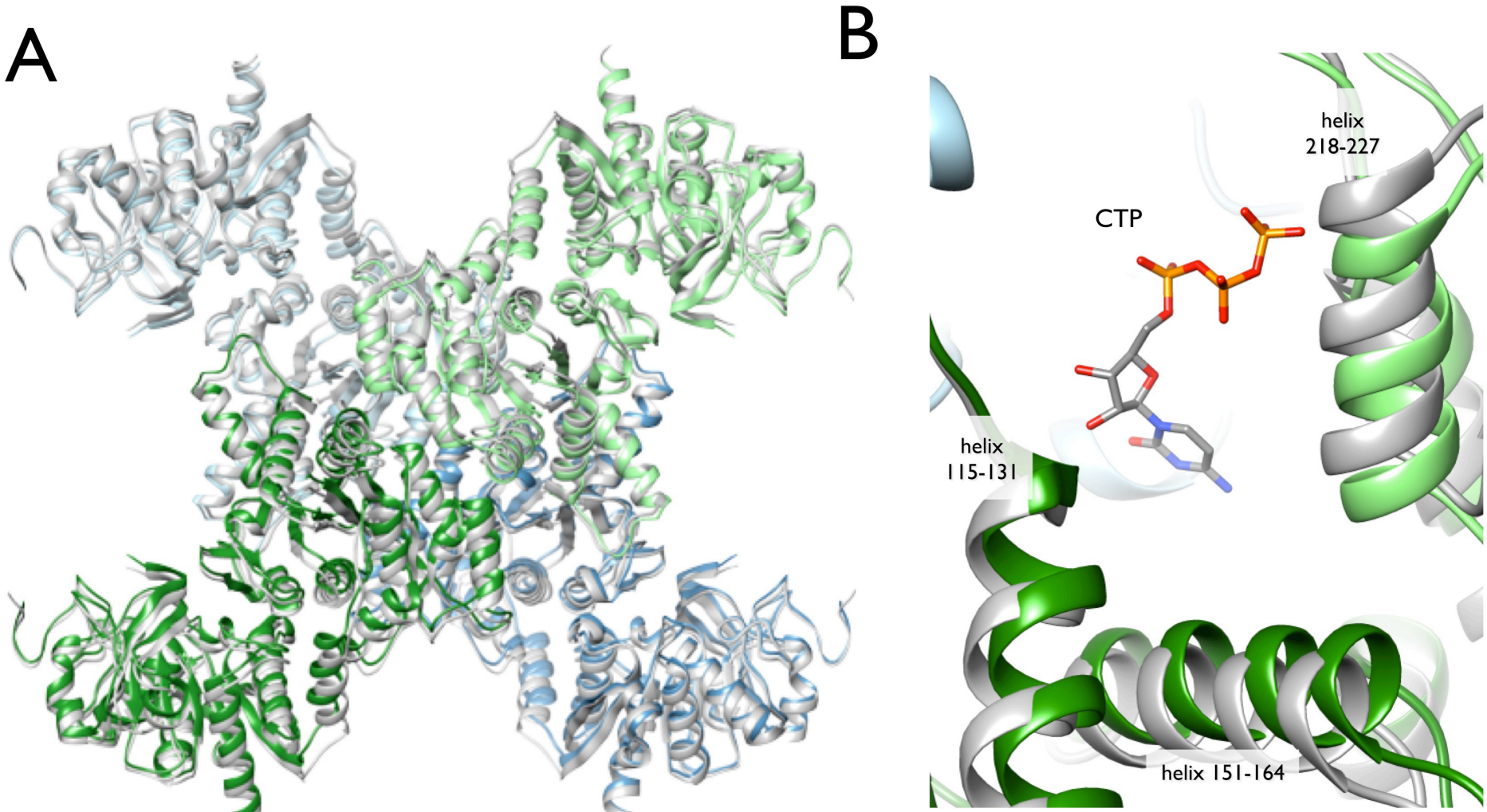

E. coli CtpS crystal structure tetramer
filament subunit

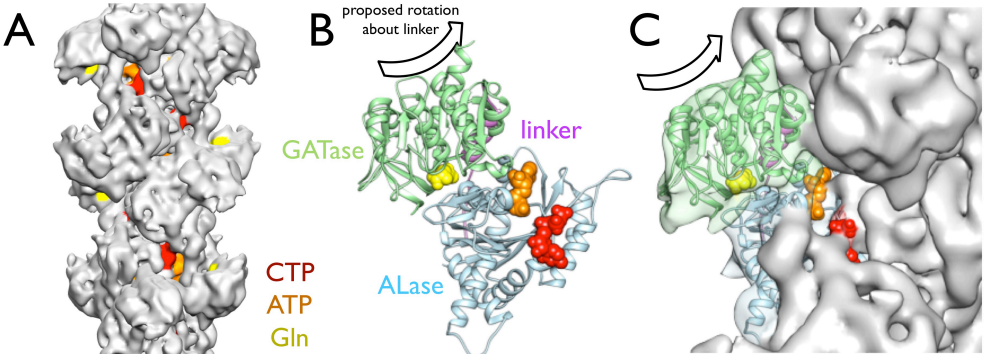
A
B
C
proposed rotation
about linker
GATase
linker
ALase
CTP
ATP
Gln

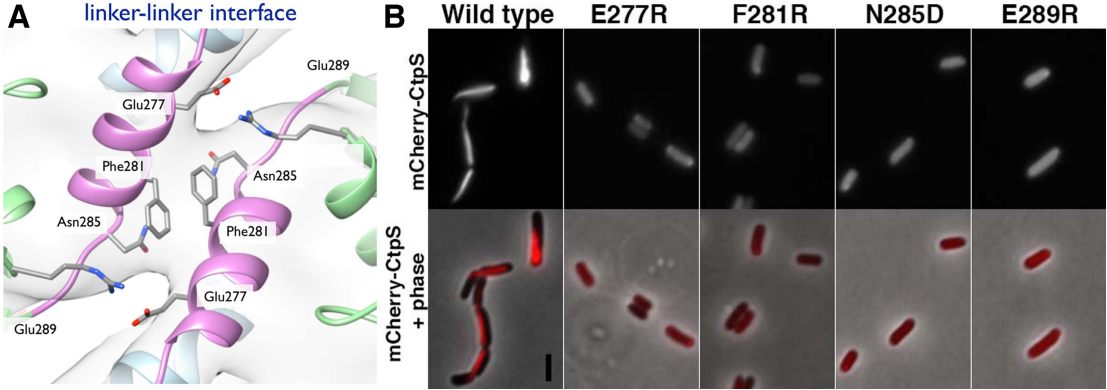
A
linker-linker interface
Glu289
Glu277
Phe281
Asn285
Asn285
Phe281
Glu277
Glu289
B
Wild type
E277R
F281R
N285D
E289R
mCherry-CtpS
mCherry-CtpS + phase

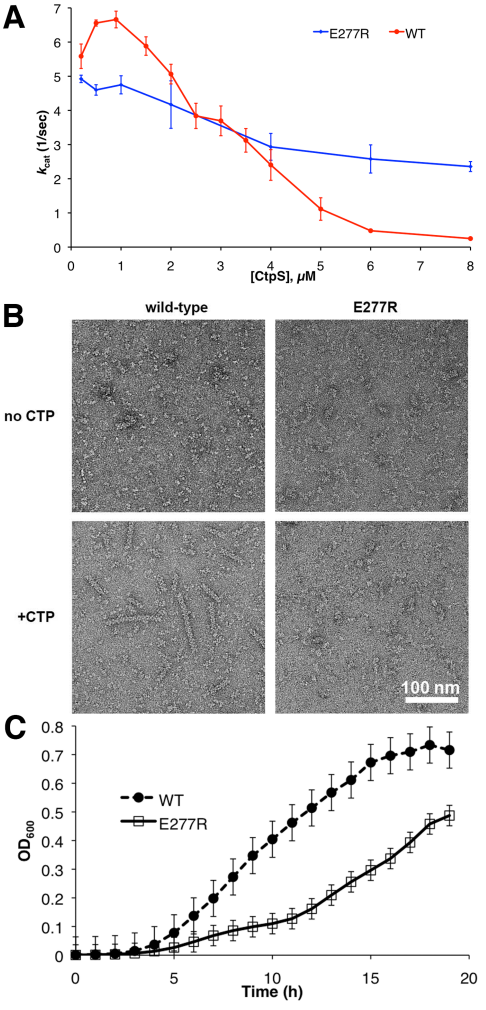
A
E277R
WT
k_{cat} (1/sec)
[CtpS], μM
B
wild-type
E277R
no CTP
+CTP
100 nm
C
WT
E277R
OD_{600}
Time (h)

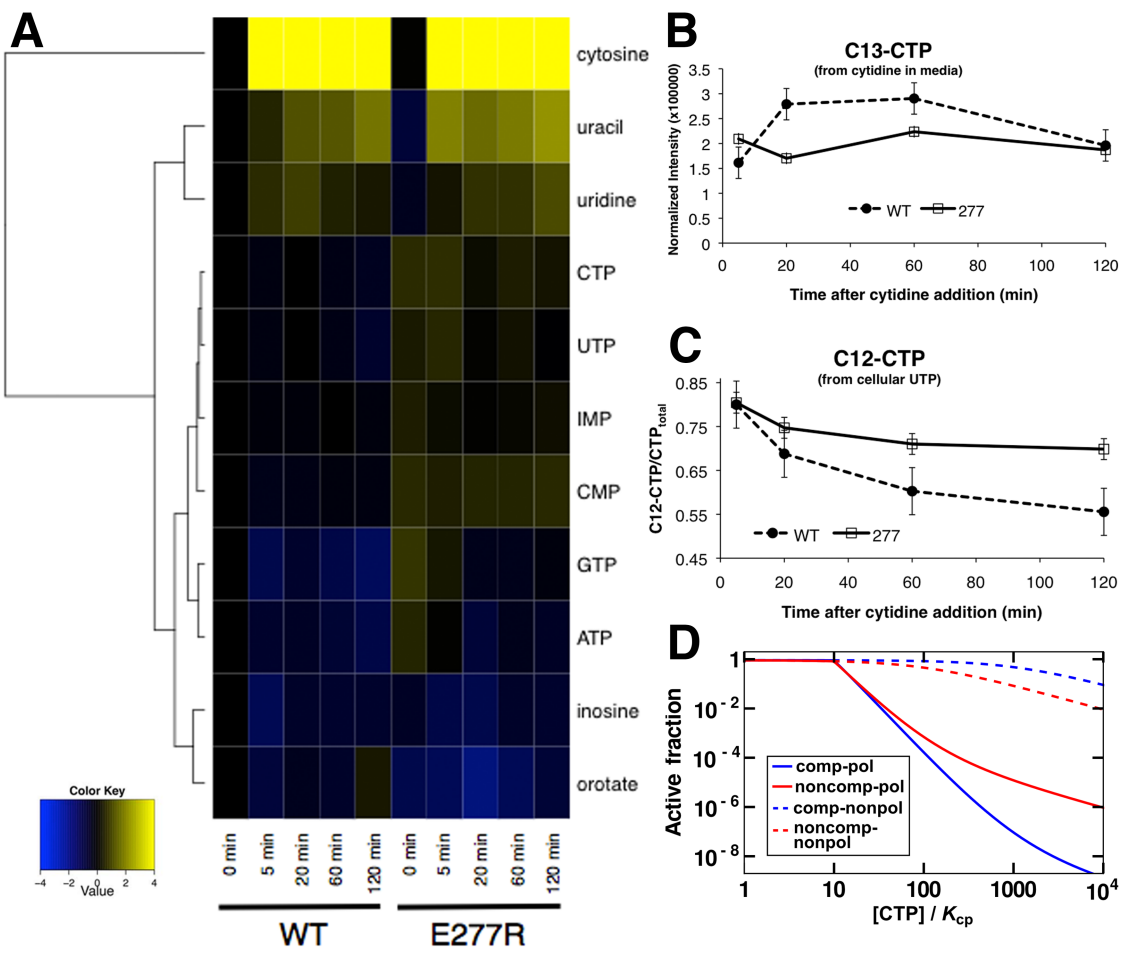
A
cytosine
uracil
uridine
CTP
UTP
IMP
CMP
GTP
ATP
inosine
orotate
Color Key
Value
0 min
5 min
20 min
60 min
120 min
WT
E277R
B
C13-CTP
(from cytidine in media)
Normalized Intensity (x100000)
WT
277
Time after cytidine addition (min)
C
C12-CTP
(from cellular UTP)
C12-CTP/CTP total
Time after cytidine addition (min)
D
Active fraction
comp-pol
noncomp-pol
comp-nonpol
noncomp-nonpol
[CTP] / Kcp

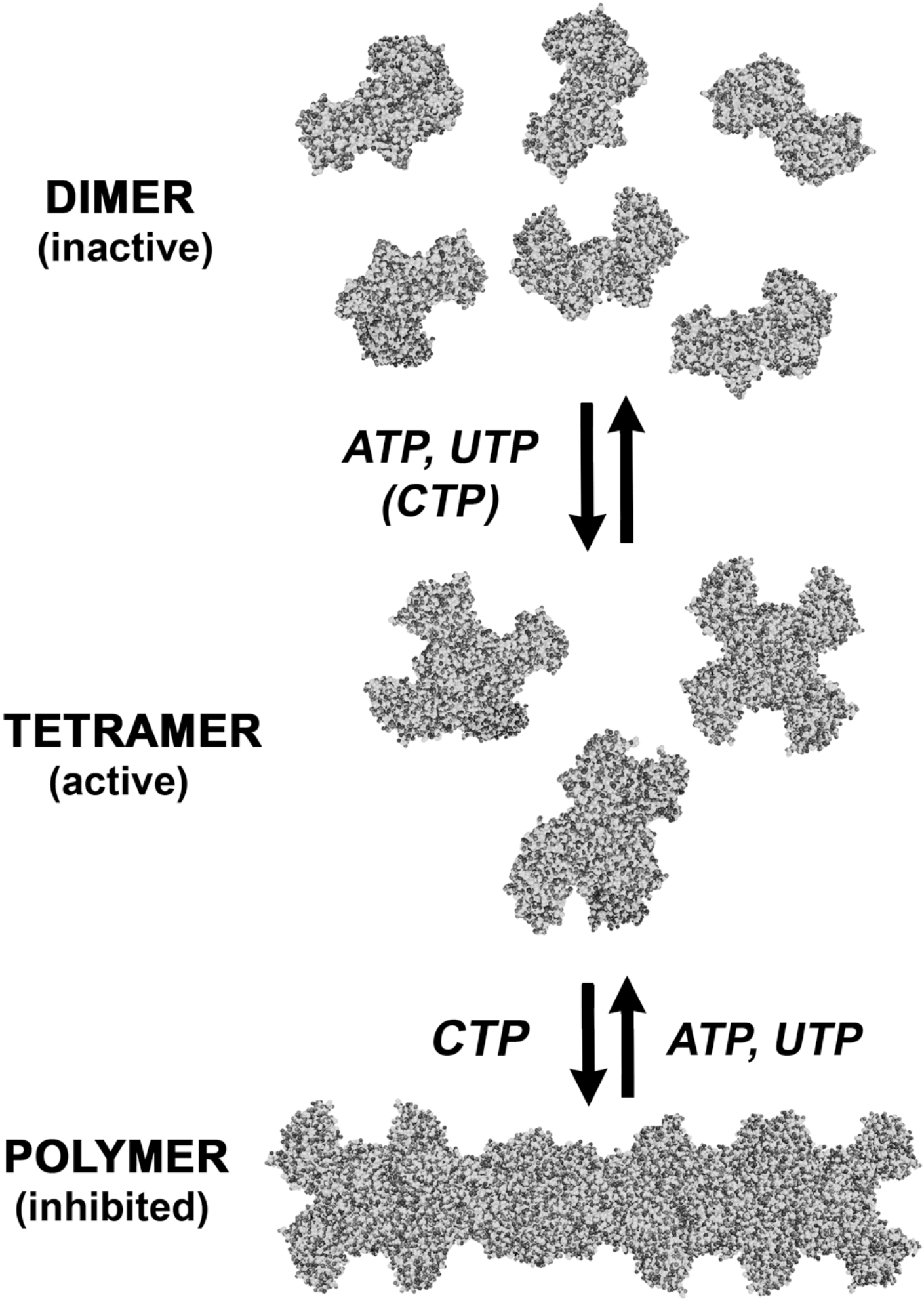
DIMER
(inactive)
ATP, UTP
(CTP)
TETRAMER
(active)
CTP
ATP, UTP
POLYMER
(inhibited)